Meteorology and Atmospheric Physics (2024) 136:10
https://doi.org/10.1007/s00703-024-01007-1

ORIGINAL PAPER

El Niño Southern Oscillation (ENSO) and Indian Ocean Dipole (IOD) signatures in tropical ozone in the Upper Troposphere Lower Stratosphere (UTLS)

Oindrila Nath[1,3] · Bhupendra Bahadur Singh[2] · Ravi Kumar Kunchala[1]

Received: 23 March 2023 / Accepted: 30 January 2024

Abstract
This study examines the combined influence of El Niño-Southern Oscillation (ENSO) and the Indian Ocean Dipole (IOD) on Upper Troposphere Lower Stratosphere (UTLS) ozone variability. The investigation employs data from the Microwave Limb Sounder (MLS) aboard the Aura Satellite and the European Centre for Medium-Range Weather Forecasts (ECMWF) ERA5 reanalysis, spanning the period 2005–2020 across tropical latitudes (20º N–20º S). Three specific events were chosen for analysis: a strong La Niña event in 2010, the co-occurrence of El Niño and moderate IOD in 2015, and a robust IOD event in 2019. During years marked by the simultaneous occurrence of ENSO and IOD events, the UTLS (100 hPa altitude is considered for the present study. 82 hPa is the altitude just above the tropopause, therefore also shown in the results) ozone mixing ratio demonstrates a decline in absolute values. The Quasi-biennial Oscillation (QBO) was also investigated, revealing a synchronized variation with the ozone anomaly in the UTLS region. Furthermore, the calculated eddy heat flux, utilized as a proxy for the Brewer–Dobson Circulation (BDC), aligns with the UTLS ozone anomalies, indicating a positive (negative) anomaly during periods of intense tropical downwelling (upwelling). To quantitatively elucidate the contributions of ENSO, IOD, and QBO to the observed ozone anomaly, a multivariate linear regression analysis was executed utilizing the least square method. The findings underscore that a notable fraction—about one-fourth of the observed UTLS ozone anomaly within the study timeframe (2005–2020) can be attributed collectively to ENSO, IOD, and QBO. This preliminary exploration underscores the substantial role played by large-scale climate drivers emanating from the Pacific and Indian oceans in shaping UTLS ozone distribution. These insights emphasize the significance of considering these climatic influences when examining the intricate dynamics and variability of UTLS ozone patterns.

1 Introduction

UTLS ozone concentration is mainly regulated by stratosphere–troposphere exchange processes and dynamics and chemistry. The highest ozone mixing ratios are found in the stratosphere, which protects Earth's surface from harmful ultraviolet radiation (Dessler 2000). Although the chemical production of stratospheric ozone determined by a balance between production and loss cycles (e.g., Portmann et al. 2012) is well known, changes in tropical UTLS ozone concentrations are influenced by dynamical processes, namely, the BDC, the QBO, and large-scale teleconnections, e.g., ENSO (Fueglistaler et al. 2009; Dessler et al. 2013). The "upwelling" is part of the BDC, which is mainly a stratospheric phenomenon (Brewer 1949; Butchart 2014). Ozone is primarily produced over the tropics due to higher solar insolation but gets transported to higher latitudes by the BDC (Plumb 2002; Birner and Boenisch 2011). QBO is the shift in zonal wind pattern in the tropical lower stratosphere and has an average period of 28 months (Baldwin et al. 2001). It has two phases—easterly and westerly where in the QBO can modulate the tropospheric (e.g., Holton and Tan 1980) upwelling over the tropics due to BDC (Flury et al. 2013). Studies have shown that the tropical convection

Responsible Editor: Clemens Simmer, Ph.D.

✉ Oindrila Nath
oindrila.nath27@gmail.com

[1] Centre for Atmospheric Sciences, Indian Institute of Technology Delhi, Hauz Khas, New Delhi 110016, India

[2] Centre for Climate Change Research, Indian Institute of Tropical Meteorology (Ministry of Earth Sciences), Pune 411 008, India

[3] Royal Belgian Institute for Space Aeronomy (BIRA-IASB), Avenue Circulaire 3, 1180 Brussels, Belgium

Published online: 06 March 2024

associated with the ENSO affects the vertical exchange of energy, moisture, momentum, and chemical constituents (Dessler et al. 2013). Despite low ozone concentration at 100 hPa in the UTLS, ozone variability plays an important role in modulating background temperatures, which modulates the stratosphere–troposphere exchange (STE) processes and stratospheric chemistry. The UTLS region also plays a significant role in regulating the stratospheric hydration–dehydration and chemistry (Forster Piers and Shine 2002; Ploeger et al. (2013); ; Singh et al. 2021; Poshyvailo-Strube et al. 2022). The ENSO and the IOD are both coupled atmosphere–ocean phenomena covering the tropical Pacific and Indian Ocean, respectively. As pointed out in the paper, both phenomena are associated with changes in regional sea surface temperatures (SSTs) in the tropical Pacific and Indian Ocean (e.g., Saji et al. 1999). IOD shows positive and negative phases (e.g., Saji et al. 1999). ENSO and IOD may regionally impact surface weather and climate by enhancing convective activity in a variety of regions, including Northern India, the Tibetan Plateau, and the Northern part of the Bay of Bengal (Legras and Bucci 2020). Also, the QBO is a major mode of variability of the tropical stratosphere and modulates BDC upwelling and the distributions of trace gases in the UTLS (Plumb and Bell 1982; Diallo et al. 2022). In the zonal mean, El Niño warms the troposphere and cools the tropical lower stratosphere (Mitchell et al. 2015). The cooling of the lower stratosphere is associated with a strengthening tropical upwelling of the BDC (relevant for Sect. 3.2) and thereby with decreasing tropical lower stratospheric ozone (relevant for the present study) which can feedback on the upwelling (Randel et al. 2021; Ming and Hitchcock 2022).

Despite the known influence of these signals on UTLS ozone, the signals from the Indian Ocean (IO) have never been explored. One such significant mode of variability is the Indian Ocean Dipole (IOD) which affects the tropical circulation and tropospheric temperatures (Lu et al. 2018; Pillai et al. 2010). The zonal gradient of sea surface temperature (SST) from the tropical western IO (50–70° E, 10° S–10° N) to the tropical south-eastern IO (90–110° E, 10° S-equator) computed as in SST anomalies between these two regions are known as IOD (Saji et al. 1999; Webster et al. 1999). A positive IOD is recognized by strong positive SST anomalies in the western IO and negative SST anomalies in the south-eastern IO (Saji et al. 1999). El Niño and IOD are concurrent quite often and have been studied extensively (Annamalai et al. 2003; Gualdi et al. 2003; Lau and Nath 2023; Li et al. 2003), though they have a complex connection rather than a simple linear relationship. The positive years of IOD are associated with increased tropospheric temperature and vertical transport which can affect the tropospheric water vapor fluxes and other tracers. Therefore, the Indian Ocean coupled mode of variability should be considered while addressing the UTLS ozone variability. Both the ENSO and the IOD are related atmosphere–ocean phenomena that affect the tropical Pacific and Indian Oceans, respectively. By boosting convective activity in a number of areas, such as Northern India, the Tibetan Plateau, and the Northern section of the Bay of Bengal, ENSO and IOD may have a regional influence on surface weather and climate (Legras and Bucci 2020; Bucci et al. 2020). The BDC upwelling and the distributions of trace gases in the UTLS are both affected by the QBO, which is also a significant mode of variability of the tropical stratosphere (Plumb and Bell 1982; Diallo et al. 2022). According to Mitchell et al. (2015), El Niño warms the troposphere in the zonal mean while cooling the tropical lower stratosphere. According to Randel et al. 2021, Ming and Hitchcock 2022, and other researchers, the tropical lower stratospheric ozone is associated with the cooling of the lower stratosphere, because it can feedback on the tropical upwelling of the BDC.

In the present study, we include the IOD signals and explore the combined effect of BDC, QBO, ENSO, and IOD on the UTLS ozone variability over the tropics. Several studied explored the contribution of ENSO on the ozone variability on global and regional basis (Zerefos et al. 1992; Steinbrecht et al. 2003; Harris et al. 2008; Rieder et al. 2013; Knibbe et al. 2014; Zou et al. 2005; Randel et al. 2009; Lee et al. 2010; Kumar et al. 2021). Krzyścin (2016) showed that the combined effect of ENSO and IOD induces ± 2% month-to-month oscillations in the equatorial, mid and even high latitudinal regions. In higher latitudes, IOD contribution is found to be more than that of ENSO. However, the study hypothesized that over the equatorial region, strong ENSO and IOD influence the ozone distribution via the BDC. The QBO is also the dominant signal in temperature in the tropical lower stratosphere and modulates the strength of the BDC and trace constituents in the tropical stratosphere (Randel et al. 2006).

The study uses pressure as the "altitude" scale, which is a widely used notion. However, negative ozone trends just above the tropopause (that are noted in a pressure-based analysis) largely vanish when a coordinate transformation is carried out to investigate tropical ozone trends relative to the tropopause height, both for ground-based and space-based observations (Thompson et al. 2021; Bognar et al. 2022). Additionally, only a small number of studies (such as Konopka et al. 2009; Fadnavis et al. 2023; Vogel et al. 2023) employ potential temperature as an alternative to pressure. The present study uses long-term satellite datasets from Aura MLS to understand the tropical UTLS ozone

variability and associated influence from the BDC, QBO, ENSO, and IOD. In this work, we have attempted to examine the tropical UTLS ozone from the ENSO–IOD combined tropical ocean perspective. We have also analyzed the QBO and tropical upwelling for a plausible explanation of the tropical UTLS ozone variations with the combined effects of Pacific and Indian Ocean signals. Our study is the first to report such a kind of ozone variation from an overall view by taking all the natural oscillations into account.

2 Data and methodology

2.1 Microwave Limb Sounder measurements for ozone mixing ratios

The Earth Observing System (EOS) Microwave Limb Sounder (MLS) is one of the four instruments onboard NASA's EOS Aura satellite, NASA's A-train group of Earth-observing satellites, launched on 15 July 2004 (Randel et al. 2006; Manney et al. 2005). MLS uses microwave emission to measure stratospheric temperature, and upper tropospheric constituents. MLS also has a unique capability to measure upper tropospheric water vapor in the presence of tropical cirrus, and also the cirrus ice content. The overall scientific objective of MLS is to help improve understanding and assessment of ozone depletion, climate change, tropospheric ozone, and volcanic effects on ozone and climate change.

The MLS makes measurements of atmospheric composition, temperature, humidity, and cloud ice globally both day and night. It observes thermal microwave emission from Earth's "limb" (the edge of the atmosphere) viewing forward along the Aura spacecraft flight direction, scanning its view from the ground to~90 km every 25 s. Aura is in a near-polar 705 km altitude orbit. As Earth rotates underneath it, the Aura orbit stays fixed relative to the sun to give daily global coverage with~13 orbits per day. MLS Measurements are performed along the sub-orbital track, and resolution varies for different parameters—5 km cross-track × 500 km along-track × 3 km vertical are typical values. The resolution and accuracy of MLS v5 ozone is given below:

Pressure / hPa	Resolution Vert. × Horiz.	Precision[a] ppmv	Precision[a] %	Accuracy[b] ppmv	Accuracy[b] %	Comments
≤ 0.0005	—	—	—	—	—	Unsuitable for scientific use
0.001	7 × 650	3.4	> 40	0.9	30	Requires averaging
0.002	6 × 450	2.5	> 40	0.4	20	Requires averaging
0.005	5.5 × 350	1.7	> 200	0.3	25	Requires averaging
0.01	5.5 × 300	1.1	> 500	0.1	100	Requires averaging
0.02	5.5 × 300	0.7	> 100	0.15	40	Requires averaging
0.05	5.5 × 400	0.4	50	0.1	15	
0.10	4 × 450	0.4	40	0.1	10	
0.21	3 × 500	0.4	30	0.1	8	
0.46	3.5 × 600	0.3	20	0.2	10	
1	3× 500	0.2	7	0.3	10	
2	3.5 × 500	0.15	3	0.3	7	
4.6	3 × 500	0.15	2	0.4	7	
10	3 × 500	0.1	2	0.4	6	
21	2.5 × 400	0.1	2	0.25	5	
46	2.5 × 350	0.06	3	0.2	8	
68	2.5 × 350	0.04	4	0.1	7	
100	2.5 × 300	0.04	20–30	[+0.005 + 7%]		
150	2.5 × 400	0.03	5–100	[+0.005 + 7%]		
215	3 × 400	0.02	5–100	[+0.01 + 10%]		
261	3.5 × 450	0.03	5–100	[+0.02 + 10%]		See note [c]
316	2.5 × 500	0.04	—	—	—	Not recommended
1000–464	—	—	—	—	—	Not retrieved

MLS has been giving data since August 2004. In this study, we have used MLS v5 ozone volume mixing ratios and temperature values for the period 2005–2020. MLS ozone useful data range is 261–0.02 hPa, and for temperature, it is 261–0.001 hPa.

2.2 ERA5 datasets for calculating the Eddy Heat Flux

ERA5 is produced using 4D-Var data assimilation and model forecasts in CY41R2 of the ECMWF Integrated Forecast System (IFS), with 137 hybrid sigma/pressure (model) levels

in the vertical and the top-level at 0.01 hPa. Atmospheric data are available on these levels and that they also are interpolated to 37 pressure, 16 potential temperatures, and 1 potential vorticity level(s).

The data are archived in the ECMWF data archive (MARS) and a pertinent subset of the data, interpolated to a regular latitude/longitude grid, and used for the analysis in this study. More details about ERA5 can be found in Hersbach et al. (2020). The eddy heat flux in the lower stratosphere is equivalent to the vertical component of the Eliassen–Palm flux (EP flux) and often used as a proxy for BDC (Andrews et al. 1987; Newman et al. 2001).

The direction and amplitude of EP Flux, a vector variable having non-zero components in the latitude-height plane, determine the relative significance of eddy heat flux and momentum flux. Meridional heat flux is the name of eddy fluxes that move heat and momentum meridionally, or from the tropics to the poles (Eliassen and Palm 1961). The influence of transient and stationary eddy fluxes on the zonal-mean circulation is frequently conceived of as being represented by Eliassen–Palm (EP) fluxes (Dwyer and O'Gorman 2017). Eliassen–Palm (EP) flux convergence best captures the planetary wave action driving the BDC. The easterly momentum deposited to slow the westerly zonal flow in winter is measured by the convergence of the EP flux in the stratosphere (Newman et al. 2001). The meridional or residual circulation must subsequently be started to achieve geostrophic equilibrium (Andrews et al. 1987). A measure of the vertical propagation of planetary waves from the troposphere is the vertical component of the EP flux vector, Fz, which is proportional to the eddy heat flux, $v'T'$. Variations in the BDC driving are usually described by any of them—the EP flux convergence and the eddy heat flux. We have used ERA5 temperature, and meridional winds (T and v) for our present study to calculate eddy heat flux which is used to represent the BDC. Monthly mean of T and v has been used for the same for the duration 2005–2020.

2.3 ENSO Niño3.4 index, IOD index, and QBO winds

In the present study, ENSO time series is calculated based on the Niño3.4 Index which has been obtained from the NOAA ERSST v5 available at CPC (see https://psl.noaa.gov/data/). The index is obtained by averaging the monthly SST anomalies over the East Central Tropical Pacific (170°–120°W, 5° S–5° N). The strength of IOD is usually denoted by the Dipole Mode Index (DMI) calculated over the Indian Ocean. The time series of monthly anomalous SST gradient between the western equatorial Indian Ocean (50°–70° E, 10° S–10° N) and the south-eastern equatorial Indian Ocean (90°E-110°E, 10°S-0°N) is obtained for this purpose (see https://psl.noaa.gov/gcos_wgsp/). We refer to the positive (negative) IOD as and when the DMI is positive (negative). The strength of QBO is denoted by the standardized 50 mb zonal wind index available at CPC (see https://www.cpc.ncep.noaa.gov/data/indices/). We have used monthly standardized data for this purpose.

3 Results

3.1 UTLS ozone, ENSO, IOD, and QBO: the teleconnection

Figure 1 illustrates the time series data for tropical UTLS ozone, as well as indices for the ENSO, IOD, and QBO. In the top panel of Fig. 1, monthly ozone anomalies are depicted, averaged across the tropical region (0°–360° E, 20° S–20° N), calculated from Aura-MLS ozone observations. These ozone anomalies are derived by subtracting the mean from individual months within the 2005–2020 timeframe. Further analysis was conducted on ozone anomalies at two distinct pressure levels, specifically 100 hPa and 82 hPa, as presented in the second and third panels of Fig. 1. The subsequent observation period encompasses notable occurrences, such as negative ozone anomalies at 100 hPa during 2010–11 and 2015–16. An intriguing observation emerges during the latter part of 2010 and early months of 2011, where ENSO and IOD exhibit a negative phase, contrasting with a positive ozone anomaly peak. Simultaneously, the zonal wind pattern, represented by QBO in the bottom panel of Fig. 1, showcases a positive response. In a contrasting scenario during the subsequent time frame (late 2015 and early 2016), both ENSO and IOD shift to a positive phase, aligning with a positive ozone phase. Meanwhile, QBO indicates a negative, westward phase. Notably, the year 2019 marked a significant positive IOD event, documented as one of the strongest on record (Lu et al. 2020; Ratna et al. 2021). Despite the event's prominence and a mildly positive ENSO Index, the ozone anomaly at 100 hPa did not exhibit considerable variation in 2019. Through comprehensive time series analysis, it becomes evident that the fluctuations in tropical UTLS ozone over the observed period are intricately linked to large-scale phenomena, predominantly driven by the interplay between ENSO and IOD. This recognition prompts a quantitative assessment of the influence of these oscillations on tropical UTLS ozone variability.

3.2 Relation of the eddy heat flux with the observed ozone variation

We further utilized Eddy Heat Flux (EHF) as a proxy to explain the BDC (Weber et al. 2011). The relative importance of eddy heat flux and momentum flux is determined by the magnitude and direction of EP Flux, a vector variable in the latitude-height plane with non-zero components. According to Eliassen and Palm (1961), eddy fluxes that transport heat and

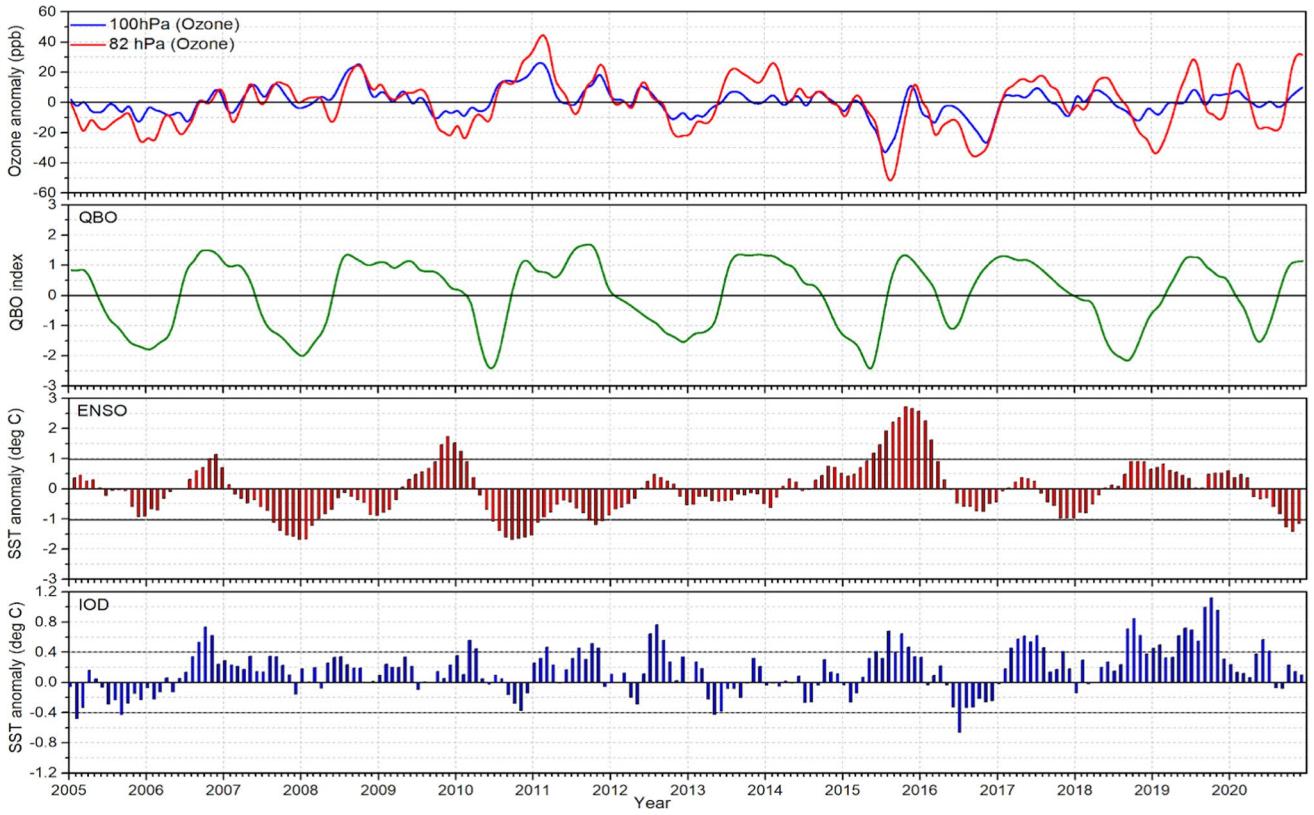

Fig. 1 Time series of MLS ozone anomaly at 100 and 82 hPa, and standardized ENSO, IOD, and QBO indexes for the time period 2005–2020. Top panel shows ozone anomaly, and QBO; middle panel shows ENSO proxy, and bottom panel shows IOD proxy DMI. The dashed lines represent the years when both the ENSO and IOD were in the same phase and ozone was in the opposite phase

momentum meridionally, or from the tropics to the poles, are known as meridional heat fluxes. The vertical component of the EP flux vector, Fz, which is proportional to the eddy heat flux, $v'T'$, provides a gauge of the planetary waves' vertical propagation from the troposphere. The EP flux convergence and the eddy heat flux are two concepts that are frequently used to characterize variations in BDC driving. Eddy heat flux has been computed by taking the zonal mean of the absolute product of v' and T'. v' is the difference between the actual meridional wind and the zonally averaged meridional wind, $v\prime = v - \overline{v}$, and T' is the difference between the actual temperature and the zonally averaged temperature

$$T' = T - \overline{T}.$$

Krzyścin (2016) hypothesized strong ENSO and IOD influences the ozone distribution via BDC over the equatorial region. We have selected 3 years of events, 2010–11 (strong La Nina), 2015–16 (strong El Niño and moderate IOD), and 2019 (strong IOD). Figure 2 (top and bottom panels) show the ozone anomaly and eddy heat flux for the year 2010–2011, respectively, using the ERA5 datasets. In Figs. 2, 3 and 4 top panels, we have plotted height-time cross-section of ERA5 ozone volume mixing ratio (OVMR) [ERA5 gives ozone mass mixing ratio, and we converted that to volume mixing ratio] zonally averaged over 20° S–20° N latitudes. Figures 2, 3, 4 (bottom panels) represent the calculated eddy heat flux (which represents the BDC) over the same latitudinal belt. Weakened eddy heat flux represents weakening in BDC. It is clearly visible in all the three cases that a weakening in BDC in the lower height range resulted in succeeding ozone reduction in the higher heights. Stronger upwelling/stronger BDC transforms more ozone from troposphere to stratosphere. When we can see higher positive eddy heat flux, we can see positive ozone anomalies in the upper heights. If we compare the three event years, it seems that the reduction in BDC is higher during the years 2015–16 and 2018–19 rather than 2010–11, i.e., strong La Niña phases have lesser impact on the tropical upwelling compared to strong El Niño and strong IOD events.

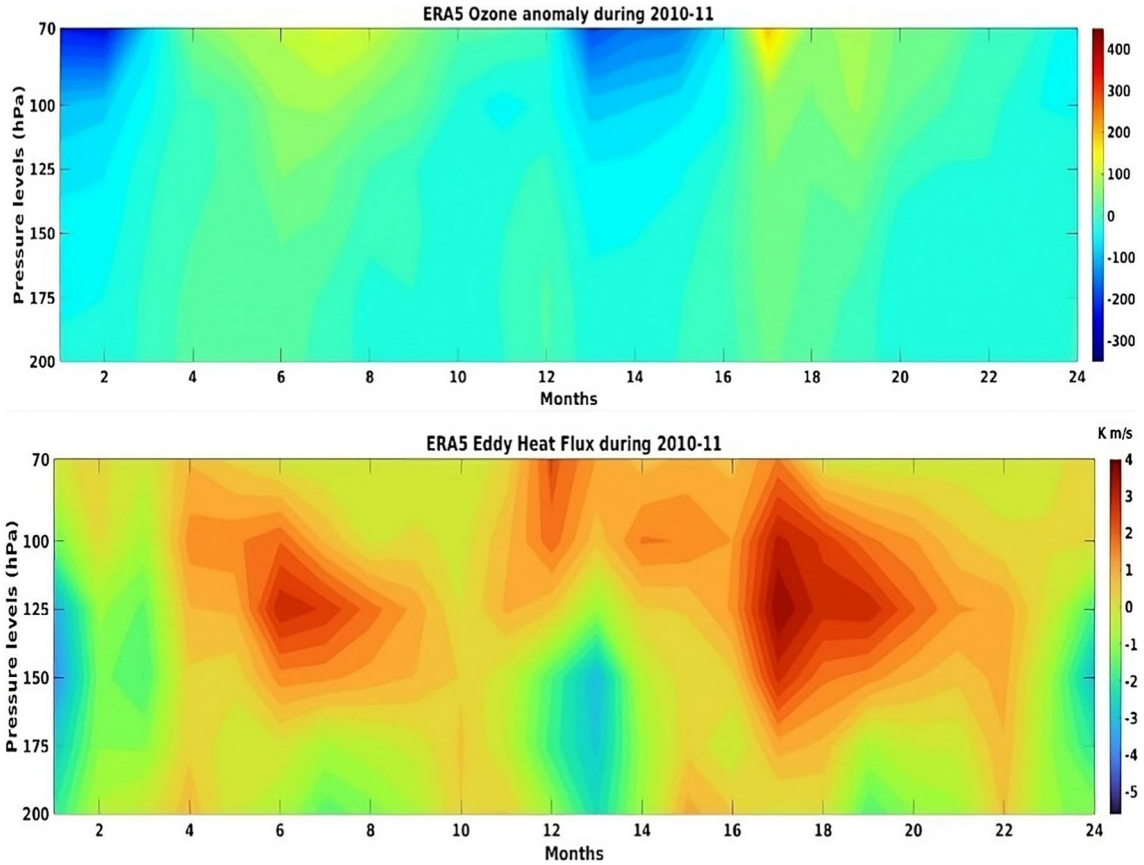

Fig. 2 (Top panel) time-height cross-section of the ozone anomaly, and (bottom panel) eddy heat flux (proxy for BDC) for the years 2010–2011

3.3 Spatial pattern of ozone, water vapor, and temperature anomalies during three different event years

Figures 5, 6 and 7 depict the spatial pattern anomalies of ozone, water vapor, and temperature, respectively, over the tropics (20°N-20°S) for the time period 2005–2020 at 100 hPa pressure level for the years 2010 (strong La Niña), 2015 (strong El Niño + moderate IOD), and 2019 (strong IOD). In Fig. 5, we can observe that the ozone anomaly is moderately positive during strong La Niña (with much higher values in the Pacific), highly positive during strong El Niño and moderate IOD (higher values in the Indian Ocean [IO]), and highly negative during strong IOD events (higher negative values over the Pacific, and mild negative over IO). During the strong La Niña event, the water vapor anomaly shows positive values over the Pacific, IO, and negative values over central Atlantic and north of South America. During strong El Niño and moderate IOD event (2015), the water vapor anomaly is moderately positive all over the tropics. And during the strong IOD event (2019), water vapor anomaly shows negative value over the Pacific but positive value over the IO. In case of temperature anomaly, we can see highly positive values over the Pacific and moderately positive values over the IO during 2010. During 2015, temperature depicts positive anomalies all over the tropics. During the strong IOD year (2019), large negative anomalies can be found over the Pacific and moderate negative values over IO. Noticeably, positive ozone and temperature anomalies are observed in part of the northern and southern Atlantic during 2019. Overall, it is quite clear from the anomaly figures that the tropical temperature is mostly modulated by the ozone concentration itself.

The potential connection between ENSO and IOD phenomena is postulated to involve the extension of the Walker Circulation toward the western regions, along with the related Indonesian throughflow—referring to the movement of warm tropical ocean water from the Pacific Ocean into the Indian Ocean. However, the visual depictions presented in the previous figures provide a qualitative overview of the influence of these large-scale circulations on tropical UTLS ozone patterns. To provide a more rigorous and quantitative understanding of the impact exerted by ENSO, IOD, and QBO events on the observed ozone anomaly, we conducted a comprehensive multivariate linear regression analysis. This analytical approach is designed

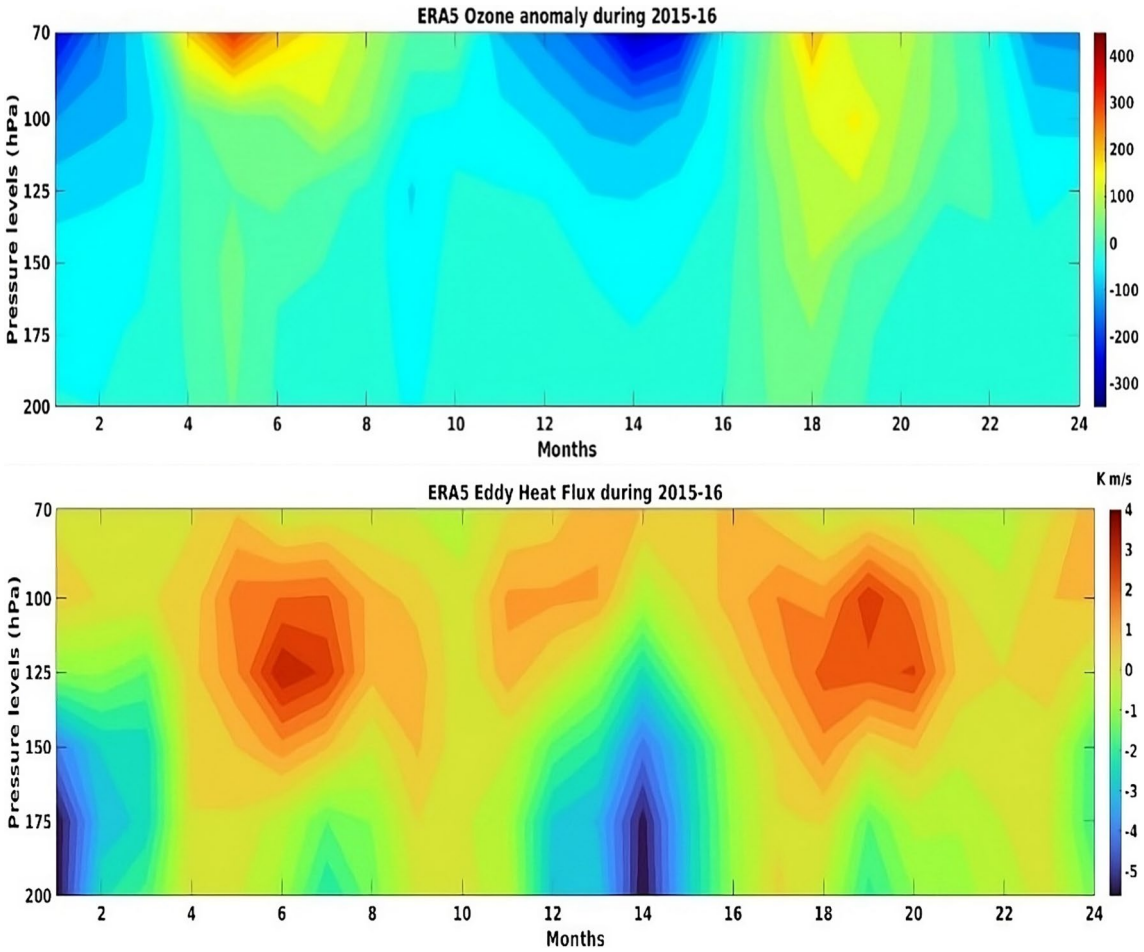

Fig. 3 Same as Fig. 2 but for the years 2015–2016

to assess the relationships and potential contributions of these distinct climate oscillations to the variations observed in ozone anomalies. The outcomes of this analysis are succinctly portrayed in the subsequent figure, offering a more systematic and data-driven perspective on the intricate interactions between ENSO, IOD, QBO events, and their collective influence on tropical UTLS ozone patterns.

3.4 Multivariate linear regression analysis of ozone anomaly

The purpose of multivariate linear regression (MLR) analysis is to regress ozone (Y) on the predictors (X) or to describe how Y depends on X (regression line or curve) $X_1, X_2, \ldots, X_k \Rightarrow$ Y. The X_i ($X_1, X_2, \ldots, X_k$) is defined as a "predictor", or "independent" variable, while Y is defined as a "dependent", "response" or "outcome" variable. Assuming a linear relation in population, mean of Y for given X equals $\alpha + \beta X$, i.e., the "population regression line". If $Y = a + bX$ is the estimated line, then the fitted $\hat{Y}i = a + bXi$ is called the fitted (or predicted) value. Therefore, in the present study, the model looks as

$$Y = B_0 + B_1.x_1 + B_2.x_2 + B_3.x_3,$$

where ozone anomaly (observed) $=> Y$; standardized ENSO index $=> x_1$; standardized IOD index $=> x_2$; standardized QBO index $=> x_3$. This is also known as the least square method. Figure 8a shows the MLR of ozone anomaly as the dependent variable with ENSO, IOD, and QBO as the components or independent variables. It is found from the model parameters that ENSO, IOD, and QBO altogether contribute to the 25% observed variation in the tropical UTLS during the period. Figure 8b depicts the individual effects of the three components separately. In Fig. 8a, we have shown the upper boundary and lower boundary for the fitted data with 95% confidence intervals. It depicts clearly that the fitted ozone gives the acceptable fit values with the considered proxies. Therefore, it also becomes clear that ENSO, IOD,

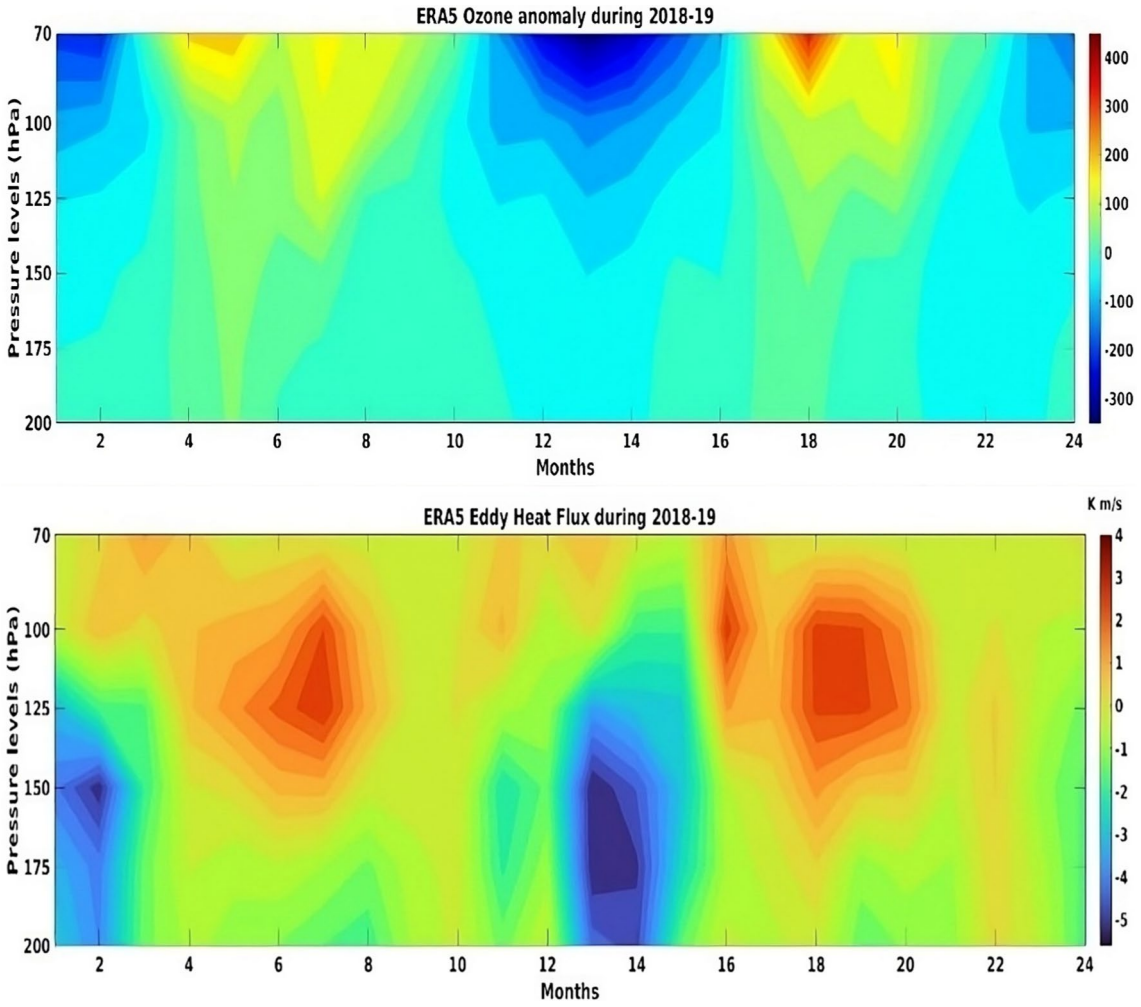

Fig. 4 Same as Fig. 2 but for the years 2018–2019

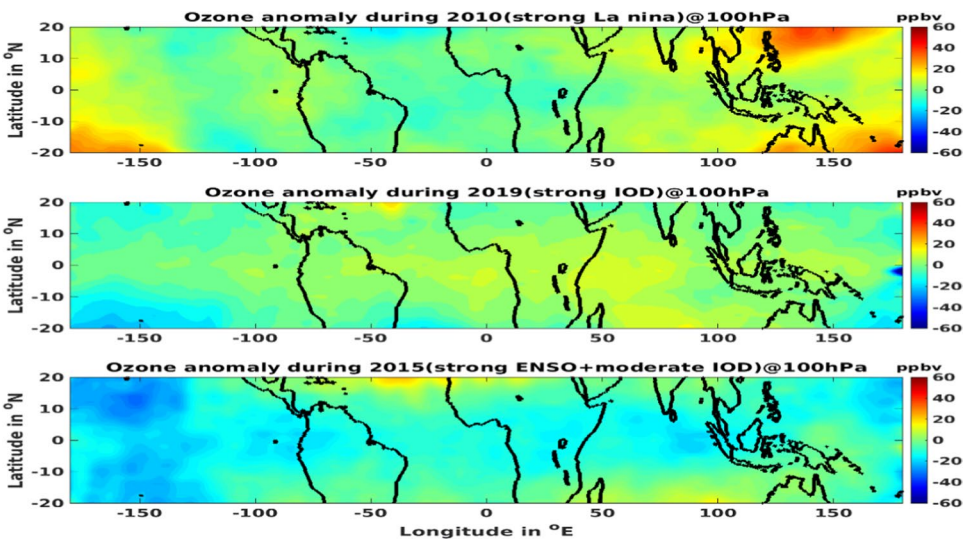

Fig. 5 Spatial pattern of ozone anomaly at 100 hPa over the tropics for the three event years of **a** only strong ENSO, **b** only strong IOD, and **c** during strong ENSO and moderate IOD events

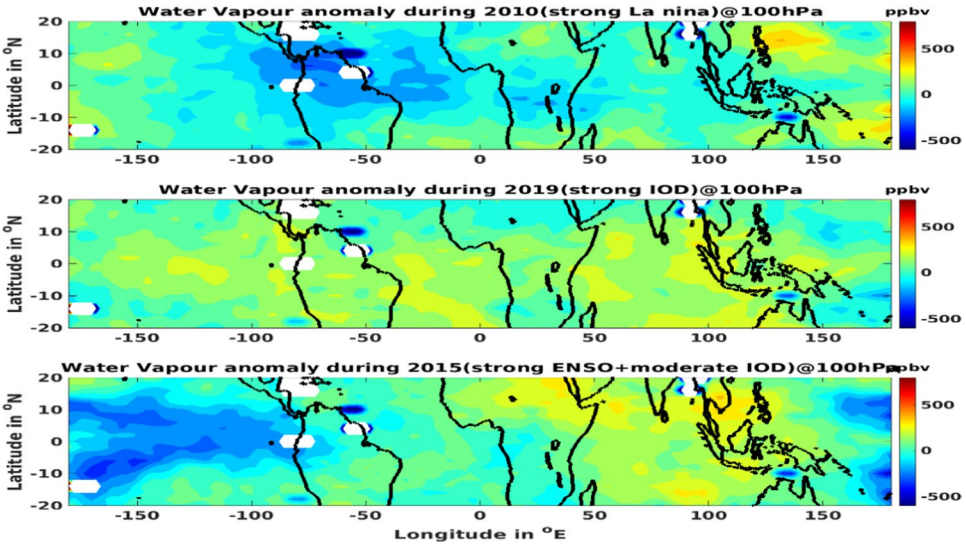

Fig. 6 Same as Fig. 5 but for water vapor

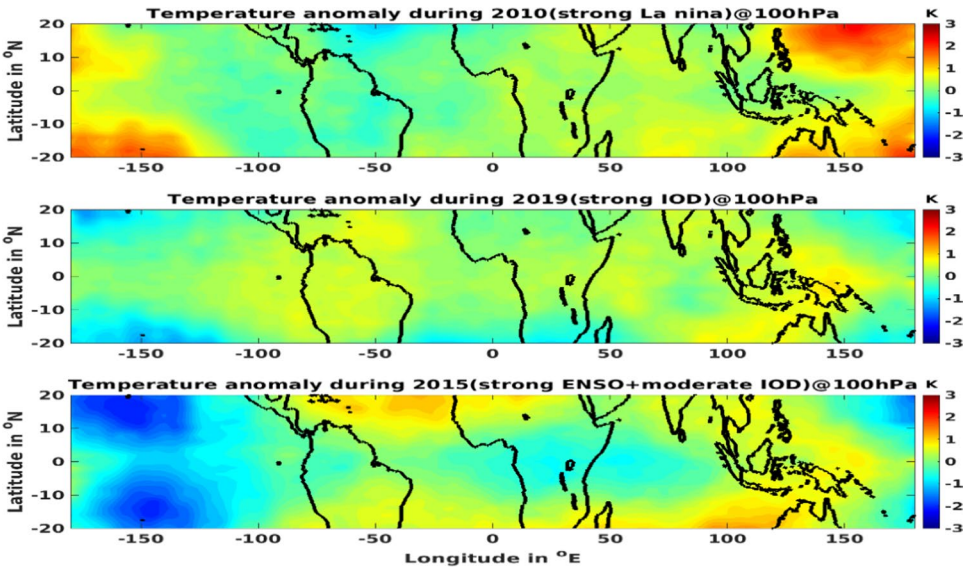

Fig. 7 Same as Fig. 5 but for temperature

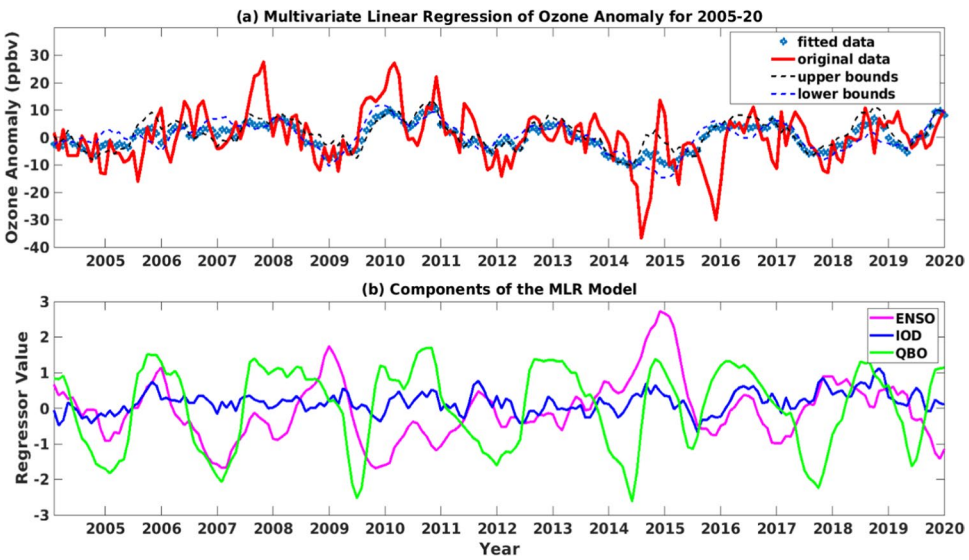

Fig. 8 **a** Observed ozone anomaly plotted with fitted ozone anomaly after multivariate linear regression analysis performed on observed ozone anomaly (dependent variable) using ENSO, IOD, and QBO as the independent variables for the time period 2005–2020 (192 months). **b** The time series of the variability for each of the components during the same time period

and QBO are having profound impact on the UTLS ozone variation.

4 Discussion and conclusion

The present study discusses the ENSO–IOD coupled effect on tropical UTLS ozone variability assessed over the period of 16 years (2005–2020). Understanding the mechanisms modulating the tropical UTLS ozone variability is important because of STE processes and the transport of ozone to the upper tropospheric heights (Davies and Schuepbach 1994), and the transport of water vapor and other gases to the lower stratosphere. We have used UTLS ozone mixing ratios (100 hPa and 82 hPa) over the tropical belt (20° N–20° S). Our study focuses on the interannual variations in relation with the combined effect of ENSO and IOD during the years (2005–2020) where we note distinct variations of ozone throughout the period. We have identified three different years with strong La Niña (2010), strong El Niño and moderate IOD (2015), and strong IOD (2019) events, and investigated the ozone anomaly during those years. We have also investigated the QBO pattern throughout the same time duration. QBO follows the ozone anomaly phase which means when the ozone anomaly is positive (negative) QBO is in positive (negative) or eastward (westward) phase. A few previous studies have discussed the ENSO effect on ozone, but this is the first time the combined and individual effect of ENSO–IOD occurrences on the UTLS ozone variability has been investigated over the tropics. Gamelin et al. (2020) showed ENSO teleconnection with UTLS ozone variability over South America. In their work, they have come up with the findings that during September–November, there are significant differences in the relationships between the ENSO teleconnections on UTLS ozone variability, and these differences depend on Pacific Decadal Oscillation phases. Our present work focuses on the tropics, we found that along with ENSO, IOD seems to show some kind of teleconnection with the UTLS ozone. Nassar et al. (2009) stated that ENSO alone shows elevated levels of tropical tropospheric ozone. In our study, when we looked into the ENSO–IOD combined effect, we found that it is negatively correlated with the UTLS ozone. To check the tropical upwelling, we also calculated the eddy heat flux and we have found that weak EHF in the lower tropospheric heights was succeeded by negative ozone anomaly near the UTLS and positive EHF brings more ozone to the UTLS, and during that time, QBO was also in eastward phase, which also favors the increase in the UTLS ozone near 100 hPa (Zhang et al. 2021). Multivariate regression analysis of the observed ozone anomaly (Fig. 8a), considering standardized ENSO, IOD, and QBO indexes as the independent variables, shows that the combined contribution of the ENSO, QBO, and IOD proxies can account for nearly one-fourth of its total variation during the analysis period (2005–2020). Although from Fig. 8b, it is clear that ENSO is having the maximum influence on the UTLS ozone anomaly compared to that of IOD and QBO, we can observe that ozone anomaly was largely negative when ENSO and IOD occurred together. This work evokes a new aspect to look into the UTLS ozone changes considering the significant links to the tropical Indian and Pacific Ocean particularly in case of co-occurrences of ENSO and IOD.

Acknowledgements The authors are thankful to the Aura-MLS team and to the European Centre for Medium-Range Weather Forecasts (ECMWF) team for providing the ozone mixing ratios, winds, and temperature datasets. The authors also thank the National Oceanic and Atmospheric Administration (NOAA) for providing the sea surface temperatures which helped to calculate ENSO and IOD indexes. The authors thank the free university of Berlin for the QBO winds data.

Data availability Nino3.4 index on: https://psl.noaa.gov/gcos_wgsp/Timeseries/Nino34/. IOD index on: https://psl.noaa.gov/gcos_wgsp/Timeseries/DMI. QBO data on: https://www.geo.fu-berlin.de/met/ag/strat/produkte/qbo/qbo.dat. ERA5 parameters on: https://cds.climate.copernicus.eu/cdsapp#!/dataset/reanalysis-era5-pressure-levels?tab=form. MLS ozone, water vapor, and temperature on: https://mls.jpl.nasa.gov.

Declarations

Conflict of interest The authors declare that they have no known competing interest. The authors declare no conflict of interest, financial interests, or personal relationships that could have appeared to influence the work reported in this paper.

References

Andrews et al (1987) middle atmosphere dynamics, 40, ISBN: 9780080511672

Annamalai H, Murtugudde R, Potemra J, Xie SP, Liu P, Wang B (2003) Coupled dynamics in the Indian Ocean: Spring initiation of the zonal mode. Deep-Sea Res 50B:2305–2330

Birner T, Boenisch H (2011) Residual circulation trajectories and transit times into the extratropical lowermost stratosphere. Atmos Chem Phys 11:817–827. https://doi.org/10.5194/acp-11817-2011

Bognar K et al (2022) Stratospheric ozone trends for 1984–2021 in the SAGE II–OSIRIS–SAGE III/ISS composite dataset. Atmos Chem Phys 22:9553–9569

Brewer AW (1949) Evidence for a world circulation provided by the measurements of helium and water vapour distribution in the stratosphere. Q J R Meteor Soc 75:351–363. https://doi.org/10.1002/qj.49707532603

Bucci S et al (2020) Deep-convective influence on the upper troposphere–lower stratosphere composition in the Asian monsoon anticyclone region: 2017 StratoClim campaign results. Atmos Chem Phys 20:12193–12210

Butchart N (2014) The Brewer-Dobson circulation. Rev Geophys 52:157–184. https://doi.org/10.1002/2013RG000448

Davies TD, Schuepbach E (1994) Episodes of high ozone concentrations at the earth's surface resulting from transport down from the

upper troposphere/lower stratosphere: a review and case studies. Atmos Environ 28(1):53–68
Dessler A (2000) Chemistry and physics of stratospheric ozone. 74, ISBN: 9780122120510
Dessler A et al (2013) Stratospheric water vapor feedback. PNAS 110:18087–18091
Diallo M et al (2022) Stratospheric water vapour and ozone response to the quasi-biennial oscillation disruptions in 2016 and 2020. Atmos Chem Phys 22:14303–14321
Dwyer JG, O'Gorman PA (2017) Changing duration and spatial extent of midlatitude precipitation extremes across different climates. Geophys Res Lett 44:5863–5871
Eliassen A, Palm E (1961) On the transfer of energy in stationary mountain waves. Geofys Publ 22(3):1–23
Fadnavis S et al (2023) Comparison of ozone sonde measurements in the upper troposphere and lower Stratosphere in Northern India with reanalysis and chemistry-climate-model data. Sci Rep 13:7133. https://doi.org/10.1038/s41598-023-34330-5
Flury T et al (2013) Variability in the speed of the Brewer-Dobson circulation as observed by Aura/MLS. Atmos Chem and Phys 13(9):4563–4575
Forster PiersShine MdFKP (2002) Assessing the climate impact of trends in stratospheric water vapor. Geo Res Lett 29(6):1086. https://doi.org/10.1029/2001GL013909
Fueglistaler S et al (2009) Tropical tropopause layer. Rev Geophys 47:RG1004. https://doi.org/10.1029/2008RG000267
Gamelin B et al (2020) The combined influence of ENSO and PDO on the spring UTLS ozone variability in South America. Clim Dyn 55:1539–1562
Gualdi S, Guilyardi E, Navarra A, Masina S, Delecluse P (2003) The interannual variability in the tropical Indian Ocean as simulated by a CGCM. Clim Dyn 20:567–582
Harris NRP et al (2008) Ozone trends at northern mid- and high latitudes—a European perspective. Ann Geophys 26:1207–1220. https://doi.org/10.5194/angeo-26-1207-2008
Hersbach H et al (2020) The ERA5 global reanalysis. Q J R Meteorol Soc 146:1999–2049
Holton JR, Tan HC (1980) The influence of the equatorial quasi-biennial oscillation on the global circulation at 50 mb. J Atmos Sci 37:2200–2208
Knibbe JS, Van Der ARJ, de Laat ATJ (2014) Spatial regression analysis on 32 years of total column ozone data. Atmos Chem Phys 14:8461–8482. https://doi.org/10.5194/acp-14-8461-2014
Konopka P, Grooß JU, Plöger F, Müller R (2009) Annual cycle of horizontal in-mixing into the lower tropical stratosphere. J Geophys Res Atmos 114:1–7
Krzyścin JW (2016) El Niño-Southern Oscillation and Indian Ocean dipole contribution to the Zonal Mean Total Ozone in the Northern Hemisphere. Int J Climatol 37:3517–3524. https://doi.org/10.1002/joc.4933
Kumar KR, Singh BB, Kumar KN (2021) Intriguing aspects of Asian Summer monsoon anticyclone ozone variability from microwave limb sounder measurements. Atmos Res 253:105479. https://doi.org/10.1016/j.atmosres.2021.105479
Lau NC, Nath MJ (2023) Atmosphere–ocean variations in the Indo-Pacific sector during ENSO episodes. J Clim 16:3–20
Lee T, Hobbs WR, Willis JK, Halkides D, Fukumori I, Armstrong EM, Hayashi AK, Liu WT, Patzert W, Wang O (2010) Record warming in the South Pacific and western Antarctica associated with the strong central-Pacific El Niño in 2009–10. Geophys Res Lett 37:L19704. https://doi.org/10.1029/2010GL044865
Legras B, Bucci S (2020) Confinement of air in the Asian monsoon anticyclone and pathways of convective air to the stratosphere during the summer season. Atmos Chem Phys 20(18):11045–11064
Li T, Wang B, Chang CP, Zhang YS (2003) A theory for the Indian Ocean dipole-zonal mode. J Atmos Sci 60:2119–2135
Lu X et al (2018) Lower tropospheric ozone over India and its linkage to the South Asian monsoon. Atmos Chem Phys 18:3101–3118. https://doi.org/10.5194/acp-18-3101-2018
Lu B et al (2020) What caused the extreme Indian Ocean dipole event in 2019? Geophys Res Lett 47(11):1–18
Manney GL et al (2005) EOS MLS observations of ozone loss in the 2004–2005 Arctic winter. Geo Res Let 33:L04802. https://doi.org/10.1029/2005GL024494
Ming A, Hitchcock P (2022) What contributes to the inter-annual variability in tropical lower stratospheric temperatures? J Geophys Res Atmos 127:e2021JD035548
Mitchell DM et al (2015) Signatures of naturally induced variability in the atmosphere using multiple reanalysis datasets. QJRMS 141(691):2011–2031
Nassar R et al (2009) Analysis of tropical tropospheric ozone, carbon monoxide, and water vapor during the 2006 El Niño using TES observations and the GEOS-Chem model. J Geophys Res 114:D17304. https://doi.org/10.1029/2009JD011760
Newman P et al (2001) What controls the temperature of the Arctic stratosphere during the spring? J Geo Res 106:19999–20010
Pillai PA et al (2010) Individual and combined influence of El Niño-Southern Oscillation and Indian Ocean Dipole on the Tropospheric Biennial Oscillation. QJRMS. https://doi.org/10.1002/qj.579
Ploeger et al (2013) Horizontal water vapor transport in the lower stratosphere from subtropics to high latitudes during boreal summer. J Geophys Res Atmos 118(14):8111–8127
Plumb RA (2002) Stratospheric transport. J Meteorol Soc Jpn 80:793–809. https://doi.org/10.2151/jmsj.80.793
Plumb RA, Bell RC (1982) A model of the quasi-biennial oscillation on an equatorial beta-plane. QJRMS 108(456):335–352
Portmann RW et al (2012) Stratospheric ozone depletion due to nitrous oxide: influences of other gases. Philos Trans R Soc B Biol Sci 367(1593):1256–1264
Poshyvailo-Strube L et al (2022) How can Brewer-Dobson circulation trends be estimated from changes in stratospheric water vapour and methane? Atmos Chem Phys 22(15):9895–9914
Randel WJ, Wu F, Vömel H, Nedoluha G, Forster PMD (2006) Decreases in stratospheric water vapor after 2001: links to changes in the tropical tropopause and the Brewer-Dobson circulation. J Geophys Res 111:D12312. https://doi.org/10.1029/2005JD006744
Randel WJ, Garcia RR, Calvo N, Marsh D (2009) ENSO influence on zonal mean temperature and ozone in the tropical lower stratosphere. Geophys Res Lett 36:L15822. https://doi.org/10.1029/2009GL039343
Randel WJ, Wu F, Ming A, Hitchcock P (2021) A simple model of ozone–temperature coupling in the tropical lower stratosphere. Atmos Chem Phys 21(24):18531–18542
Ratna SB et al (2021) The extreme positive Indian Ocean dipole of 2019 and associated Indian summer monsoon rainfall response. Geophys Res Lett 48(2):e2020GL091497
Rieder HE et al (2013) On the relationship between total ozone and atmospheric dynamics and chemistry at mid-latitudes – Part 2: The effects of the El Niño/Southern Oscillation, volcanic eruptions and contributions of atmospheric dynamics and chemistry to long-term total ozone changes. Atmos Chem Phys 13:165–179. https://doi.org/10.5194/acp-13-165-2013
Saji S et al (1999) A dipole mode in the tropical Indian Ocean. Nature 401(6751):360–363
Singh BB, Krishnan R, Ayantika DC et al (2021) Linkage of water vapor distribution in the lower stratosphere to organized Asian summer monsoon convection. Clim Dyn 57:1709–1731. https://doi.org/10.1007/s00382-021-05772-2

Steinbrecht W, Hassler B, Claude H, Winkler P, Stolarski RS (2003) Global distribution of total ozone and lower stratospheric temperature variations. Atmos Chem Phys 3:1421–1438. https://doi.org/10.5194/acp-3-1421-2003

Thompson A et al (2021) Regional and seasonal trends in tropical ozone from SHADOZ profiles: reference for models and satellite products. J Geophys Res Atmos 126(22):e2021JD034691

Vogel B et al (2023) Reconstructing high-resolution in- situ vertical carbon dioxide profiles in the sparsely monitored Asian monsoon region. Commun Earth Environ 4:72. https://doi.org/10.1038/s43247-023-00725-5

Weber M et al (2011) The Brewer-Dobson circulation and total ozone from seasonal to decadal time scales. Atmos Chem Phys 11(21):11221–11235

Webster PJ et al (1999) Coupled Ocean–atmosphere dynamics in the Indian Ocean during 1997–98. Nature 401(6751):356–360

Zerefos CS, Bais AF, Ziomas JC, Bojkov RD (1992) On the relative importance of Quasi-Biennial Oscillation and El Niño/Southern Oscillation in the Revised Dobson Total Ozone ˜ Records. J Geophys Res 97:10135–10144

Zhang J et al (2021) The role of chemical processes in the quasi-biennial oscillation (QBO) signal in stratospheric ozone. Atmos EnvIron. https://doi.org/10.1016/j.atmosenv.2020.117906

Zou H, Zhou L, Gao Y, Chen X, Li P, Ji C, Ma S, Gao D (2005) Total ozone variation between 50° and 60°N. Geophys Res Lett. https://doi.org/10.1029/2005GL024012. (**issn: 0094-8276**)